

INTERNATIONAL COUNCIL OF THE AERONAUTICAL SCIENCES (ICAS)

A NEW METHOD OF LASER VELOCIMETRY FOR AIRLOADS DETERMINATION
ON HOVERING ROTOR BLADES

Eric BERTON, Daniel FAVIER, Christian MARESCA, Marcellin NSI MBA
Institut de Mécanique des Fluides, Université d'Aix-Marseille II, UM 34 du CNRS,
Les Souffleries de Luminy, 163 avenue de Luminy, 13009 Marseille, France.

Abstract

The flowfield around hovering rotor blades with either rectangular or evolutive tip shapes is investigated in this paper. For different blade tip geometries the measurements concern local and overall aerodynamic data sets, including : the instantaneous velocity field around the blade and in its near wake and the global thrust and power coefficients. From such data sets the present paper is focused on deriving an original data post-processing method to correlate the L.V. flow measurements around the blade with the overall (C_T , C_Q) and local (C_L , C_D) airloads coefficients. This new method of determination of the overall and local airloads coefficients has been based on the Kutta and momentum equation (K.M.E.) applied to the velocity field (axial and tangential) measured along a close contour surrounding the blade section at a given blade radius. To check the capability of such a method the present paper offers a series of comparisons on overall and local aerodynamics coefficients deduced : from (C_T , C_Q) measurements performed by means of a rotative balance, and (C_L , C_D) coefficients obtained either in 2D steady flow conditions or from the K.M.E applied to the L.V. flow measurements performed around the blade.

Nomenclature

b	number of blades (b=2 ou 4)
c	constant blade chord, (c=0.05 m)
C_T	rotor thrust coefficient
C_Q	rotor power coefficient
Γ	blade circulation along the span, (m^2/s)
Oxyz	reference system defined in Fig. 3
θ	collective pitch angle at $r/R=0.75$, (deg)
θ_v	blade twist law, (deg)
r	radial distance from rotation axis, (m)

R	rotor blade radius, (R=0.75 m)
R_o	root cut out, ($R_o=0.22R$)
σ	rotor solidity ($\sigma=bc/\pi R$)
T,Q	rotor thrust and torque, (N, N.m)
u, l	upper and lower side of the blade sections
V,W	tangential and axial velocities
V_e	rotational tip speed, ($V_e=\omega R=107$ m/s)
ω, Ω	angular frequency, ($\omega=143$ rad/s)
ψ, ψ_p	blade azimuth, (deg)

Introduction

The prediction of the flowfield and the airloads repartition in the tip region of helicopter rotor blades play a major role for providing and evaluating improved rotor designs. Since the flow tip region experiences the largest amplitudes of variations in the bound circulation and the loading repartition, the adequate tip geometry modifications can lead to significant improvements in the overall rotor performances. However, the accurate prediction of the flowfield generated by sharp evolutive tip shapes still poses some problems to available numerical schemes, and requires additional research efforts using experimental investigations. This is the motivation of the present research.

MethodologyThe K.M.E. Method

Application of the Kutta and Momentum Equation method (K.M.E.) in hover, (see Figure 1), begins with the application of the momentum equation to the general control surface S surrounding the blade section at a given radial station r/R (1 to 3) :

$$-\oint_S \vec{dF}_{ext} ds = \oint_S (\rho \vec{q} \cdot \vec{n}) \cdot \vec{q} ds \quad (1)$$

The contour S is divided into three contours, $S = \Sigma_a + \Sigma_w + \Sigma$, where Σ_a , Σ_w and Σ represent the contour enveloping the airfoil section, the near wake and the external contour around the blade section. Due to the non slip condition on the airfoil surface ($\vec{q} \cdot \vec{n} = 0$), and the continuity of pressure across the wake sheet ($P_{wu} = P_{wl}$), the momentum equation can be written as :

$$-\oint_{\Sigma_a} dF_{ext} \vec{n} ds = \oint_{\Sigma} P \vec{n} ds + \oint_{\Sigma} (\rho \vec{q} \cdot \vec{n}) \cdot \vec{q} ds \quad (2)$$

What remains is a line integral about the arbitrary contour Σ surrounding the blade section. As shown in Figure 2, selecting Σ as a rectangular box ABCD of length $2\pi/b$ (where b denotes the number of blades) obviates the need to include the vertical segments BC and DA of the line integral because of cancellation due to flow periodicity. Choosing this specific contour simplifies the momentum equation such that the horizontal force component dF_y acting on the blade section can be expressed in terms of the axial and tangential velocity components along the upper and lower contour segments as follows:

$$-dF_y = \rho r \int_0^{2\pi/b} [W_l V_l - W_u V_u] d\psi \quad (3)$$

while the application of the Kutta formula provides the vertical component dF_z as :

$$-dF_z = \rho \Omega r^2 \int_0^{2\pi/b} [V_l - V_u] d\psi \quad (4)$$

The Kutta equation formulation for dF_z is more attractive than that derived from the momentum equation due to the lack of pressure terms. The above derivations show that the elementary forces (dF_y , dF_z) acting on the blade section can thus be deduced from the tangential and axial velocity components alone. The global thrust and power coefficients (C_T , C_Q) are derived by integrating the elementary forces (dF_y , dF_z) along the span as :

$$\Omega C = b \int_{R_0}^{R_1} dF_y (\Omega r) dr ; C_Q = \frac{\Omega C}{\rho \pi R^2 V_e^3} \quad (5)$$

$$T = b \int_{R_0}^{R_1} dF_z dr ; C_T = \frac{T}{\rho \pi R^2 V_e^2} \quad (6)$$

Local incidence $\alpha = \theta - \theta_i$ can also be determined from the streamlines computed from the measured velocity field in the immediate vicinity of the blade. The local section aerodynamic coefficients of lift and drag are then obtained by simple transformation of the elementary forces (dF_y , dF_z) as :

$$dL = dF_z \cos \theta_i + dF_y \sin \theta_i$$

$$C_l = \frac{dL}{1/2 \rho [(\Omega r - V_i)^2 + W_i^2]} \cdot c \quad (7)$$

$$dD = dF_y \cos \theta_i - dF_z \sin \theta_i$$

$$C_d = \frac{dD}{1/2 \rho [(\Omega r - V_i)^2 + W_i^2]} \cdot c \quad (8)$$

Rotor Model and Hovering Tests Conditions.

The model-scale of rotor (diameter : 1.50 m) is set up on the hovering test rig installed in the testing hall of the S1-Luminy wind-tunnel. The rotor hub is mounted vertically by means of a supporting mast, so that the center of rotation is located 2.90 m above the ground. The model-rotor consists of a fully articulated rotor hub which can be equipped with interchangeable sets of blades. Rotor blades definition is given in Figure 3. The different sets of rotor blades tested are numbered from 4 to 7, and correspond to various combinations of blade twist, airfoil section and tip shape. The different tip geometries : swept, tapered, parabolic and rectangular (respectively for rotors 4, 5, 6, 7) provide the same rotor solidity ($\sigma = 0.08403$ for $b = 4$).

Measurements Procedures.

Several techniques suited for surveying the flow around the blades and the flow in the near and far wake regions, have been developed including 2D-laser velocimeter and a 6-components balance. More detailed informations concerning these measurement techniques can be found in references (4 to 7), only a short description is given here.

Overall forces measurements (averaged thrust and torque) are performed by means of a 6-components balance mounted on the rotor hub.

The velocity field around the blade is measured by means of the 2D fiber optic laser velocimeter technique providing the axial and tangential velocity components along a close contour surrounding the blade section and as a function of the blade azimuthal position. Figure 4 provides a view of the tapered model rotor installation, of the LV system showing the traverse, optics, and the beam intersection forming the LV measuring volume. The overall and local airloads coefficients as well as the circulation distribution along the span are then deduced from the integration of these flow velocity measurements as described below.

Results

In the present experimental investigation, both overall and local aerodynamic quantities of the flowfield through the hovering rotor have been measured on configurations of rotors 4, 5, 6, 7, for collective pitch angles θ , and number of blades b , varying in the following ranges : $6^\circ \leq \theta \leq 10^\circ$; $2 \leq b \leq 4$.

For the purpose of the present paper, the following experimental results will be only focused on the analysis of the tip shape influence as deduced from measurements performed on the two rotors 4 and 7 (see Figure 3). Both rotors are considered at the same set of operating parameters : $b=4$ or 2 , $\theta = 10^\circ$, $\Omega R = 107$ m/s, and the blades only differ by the tip geometry, which is rectangular on rotor 7 and swept on rotor 4. Both rotors have also very close thrust coefficient : $C_T = 0.00797$ for Rotor 4, and $C_T = 0.00766$ for Rotor 7 in a four-bladed configuration.

Tangential Velocity Field Around the Blade and Bound Circulation

As previously mentioned, the tangential velocity field around the blade is determined by means of velocimetry laser measurements performed at two fixed points (u and l) on the upper and lower side of the blade section. The plots in Figure 5 present the comparison of the tangential velocity profiles, measured as a function of the blade azimuth, on the upper side $V_u = V_u(\psi)$ and the lower side $V_l = V_l(\psi)$ of the two rotor blades 4 and 7 operating at the same conditions.

For the upper side of the airfoil sections, the inversion of the sign of the tangential velocity V_u , localizes accurately the blade passage at $\psi = 45^\circ$ on both rotors. On the lower side, the V_l -

velocity profile show successively (as a function of ψ) : a first peak in the velocity evolution (corresponding to the blade passage influence on the measurement point l), and then, a second peak of velocity which reflects the influence of the vortical wake shed by the preceding blade on the measurement point l .

As shown in Figures 5, the V_u and V_l profiles relative to the swept tips of rotor 4, exhibit important fluctuations outside the blade passage influence ($30^\circ \leq \psi \leq 70^\circ$). The perturbation of the tangential velocity field between two consecutive blades is thus typical of the swept tip influence, and is not observed on the blades of the rotor 7. In this case, the tangential velocity field appears almost uniform between two blades.

It can be also noticed that the velocity fluctuations observed on rotor 4, are occurring around a mean value (in time) which is close to the constant value observed on rotor 7. These fluctuations on the tangential velocity field between two blades, has to be directly correlated to the instability of the vortex system generated by the swept tip, and significantly influences the distribution of circulation along the span as shown in Figure 6. The bound circulation on the blade is deduced from integration of the instantaneous velocity profiles V_u and V_l . For rotor 4, the results of this integration introduces a double peak evolution in the distribution $\Gamma = \Gamma(r)$ along the span (see Figure 6). The main peak, located at $r/R = 0.875$, is associated with an increase ($0.75 \leq r/R \leq 0.875$), and a decreased ($0.875 \leq r/R \leq 1$) of the bound circulation on the blade. The second peak, less intense than the previous one, is located at the radial position $r/R = 0.65$. Such a behaviour on the Γ -distribution is not observed in Figure 6 for the rectangular tips of rotor 7. In this case, when the blade is far from the point of measurement, the tangential component keeps a constant value at nearly the same level on upper and lower side. This fact involves that, outside the blade passage, the contribution of the tangential velocity to the circulation is small (the area between the two curves is almost equal to zero). For the rotor 7, the value of the circulation results principally from the area enclosed between the two curves of the tangential velocity corresponding to the blade passage ($35^\circ \leq \psi \leq 75^\circ$). Concerning the rotor 4, the profiles in the Figure 6 show that the value of circulation results from the area between the curves of tangential velocity on upper and lower

sides associated with the blade passage, and also with the region outside the blade passage.

Local Airloads and Integrated Global Performance

In this section we discuss the application of the K.M.E. method in the derivation of the local airloads along the blade span and their contributions to global rotor performance. Results are presented for both rotors 4 and 7. As described in the methodology review, the K.M.E. procedure requires axial and tangential velocity information along two horizontal contours - one above the rotor plane and one below - of length $2\pi/b$. Ideally, these contours should be located as close as possible to the rotor plane. In practice, however, there exists an optimum offset distance, denoted Z_{Σ} , for which the K.M.E. method yields consistent results. This distance is determined by conducting a series of surveys at increasing offset distances until the integrated elementary force results stabilize (see Figure 7). For the given conditions, the elementary forces dF_y and dF_z stabilize at offset distances beyond 5 mm.

The results in Figure 8 indicate that the dimension of the contour of integration has to be selected so that $|Z_{\Sigma}| \leq 25$ mm (i.e. nearly less than half a chord), to get consistent values on the elementary forces dF_y and dF_z . Thus a contour thickness of $|Z_{\Sigma}| = 15$ mm has been selected for all the present tests.

Axial and tangential velocity surveys at the prescribed offset distances were conducted along 20 spanwise stations ranging from .30R to 1.0R. Application of the K.M.E. procedure produced the radial distributions of the elemental forces, dF_y and dF_z , shown in Figure 9. Overall rotor thrust and torque were then derived by integration of the elemental force distributions along the span. The Figure 9a gives the evolution of the elementary force dF_y plotted versus the blade span as deduced from the integration of the velocity profiles (equations (3) and (5)). The results indicate that the C_Q coefficient value deduced from the 6-component balance is very close to those deduced from the L-V flow measurements and from the application of the K.M.E. method. In the same way similar results and conclusions are also obtained in Figure 9b concerning the C_T coefficient (equations (4) and (6)). In this case the difference between the thrust coefficient deduced from the K.M.E. method and

the thrust coefficient obtained by means of the 6-components balance is less than 1%.

Figure 10 illustrates another application of the K.M.E. method on the swept rotor 4. In this case, the power coefficient deduced from the momentum equation is equal to 0.000707 and the power coefficient measured by the balance is 0.000720. The difference between the two values is also less than 2%. Note also a difference less than 1% between the thrust coefficient deduced from the K.M.E. method and the thrust coefficient obtained by means of the 6-components balance.

The elementary forces acting on the blade section were derived from the velocity data contained in a single pair of L.V. surveys. Transforming these forces into local lift and drag requires considerably more velocity information. In order to deduce the local aerodynamic incidence, α , the velocity field must be mapped in sufficient detail to compute the streamlines around the blade section. An example of the L.V. grid density employed is provided by Figure 11, which shows a composite of the axial and tangential velocity measurements made at $r/R = .75$. From such instantaneous flow scanning around different spanwise stations, the streamlines and the local aerodynamic incidence are obtained as exemplified in Figure 12. A last example of the capability of the measurement method is given in Figure 13, concerning the rotor 7 at $b = 4$ and $\theta = 10^\circ$. The Figure gives a comparison between the OA209 coefficients 2D-table and the lift and drag coefficients (C_L and C_D) as deduced from the application of the K.M.E. and the B.E. methods (equations (7) and (8)). The distributions of the lift and drag coefficients deduced from the two determination procedures are shown to be in good agreement along the blade span r/R .

Conclusion

In the present study, an experimental approach has been derived to investigate the fine structure of the flowfield around hovering rotor blades. When compared to the rectangular tips, the swept tips are shown to strongly modify the tangential velocity field around the blade itself, and thus introduce a significant bound circulation perturbation. An original method to correlate the flow measurement around the blade with the overall and local airloads coefficients has been also presented in this paper.

This new method of determination of the overall and local airloads coefficients has been based on the Kutta and momentum equation applied to the velocity field measured along a close contour surrounding the blade section at a given blade radius.

The capability of such a method has been checked from a series of comparisons on overall and local aerodynamics coefficients deduced : either from (C_T, C_Q) measurements performed by means of a rotative balance, and (C_L, C_D) coefficients obtained in 2D steady flow conditions, or from the K.M.E method applied to the flow measurements performed around the blade.

Acknowledgments

The authors wish to thank the support provided by the "Direction des Recherches Etudes et Techniques" under Grants 90/169 and 92/061.

References

- (1) BERTON, E., FAVIER, D., MARESCA, C., NSI MBA, M. : "Détermination des charges aérodynamiques d'un rotor en vol stationnaire par vélocimétrie laser", Proceedings du 11ème Congrès Français de Mécanique, Vol. 2, pp. 365-368, Lille - Villeneuve d'Asq, September 1993.
- (2) SILVA, M, FAVIER, D., RAMOS, J, NSI MBA, M. and BERTON, E. : "An experimental investigation of the drag mechanisms of a helicopter rotor in hovering flight", Proceedings of 19th European Rotorcraft, Vol. 1, Paper n° 18, Cernobbio, September 1993.
- (3) RAMOS, J, NSI MBA, M., BERTON, E., FAVIER, D. and SILVA, M. : "A laser velocimetric investigation of the airloads and performance of a model helicopter rotor in hover", A.H.S., Proceedings of the Specialist Conference of the American Helicopter Society on Aeromechanics of Helicopters rotors, Vol. 1, Paper n° 8.1, San Francisco, January 1994.
- (4) NSI MBA, M., FAVIER, D., MARESCA, C., CRESPI, P. : "Helicopter rotor wake investigation using a laser doppler velocimeter technique", I.S.A.L.A., Proceedings of fourth International Symposium on Application of L.D.A. to Fluid Mechanics, Lisbon, July 1988.

- (5) FAVIER, D., MARESCA, C., BERTON, E. and PLANTIN DE HUGUES, P. : "Investigation of the Tip Shape Influence on the Flowfield Around Hovering Rotor Blades", A.I.A.A., 22nd Fluid Dynamics, Plasma Dynamics and Laser Conference, Honolulu, June 1991.
- (6) FAVIER, D., MARESCA, C., BERTON, E. and PLANTIN DE HUGUES, P. : "Investigation of the Flowfield Around Rotor Blade Tips in Hover", COBEM, 11th Brazilian Congress of Mechanical Engineering, Sao Paulo, December 1991.
- (7) BERTON, E. : "Contribution à l'Etude de l'Écoulement Induit Autour et dans le Sillage de Surfaces Portantes en Rotation. Application au Rotor d'Hélicoptère en Vol Stationnaire.", Thèse de Doctorat, Université d'Aix-Marseille II, I.M.2., I.M.F.M., Septembre 1992.

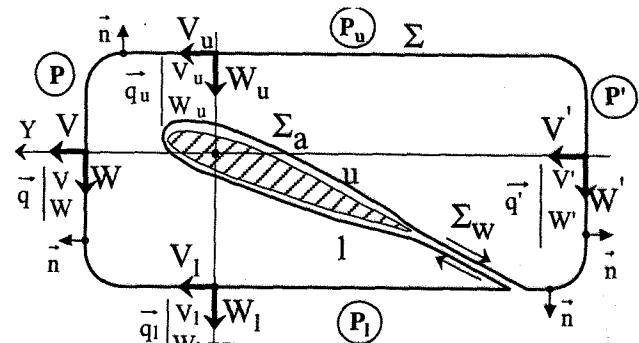


Fig.1. - General control surface around blade section

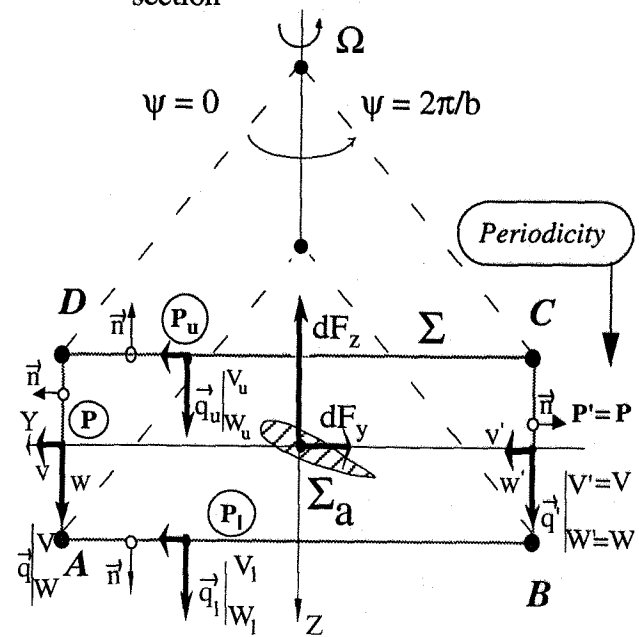
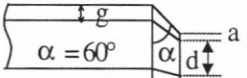
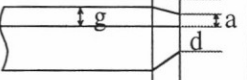
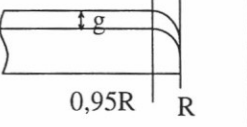
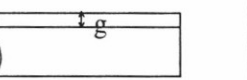


Fig.2. - Specific contour for hovering rotor

Rotor Number	Twist	Planform	Airfoil
4	-8,3°		OA209
5	-8,3°		OA209
6	-8,3°		OA209
7	-8,3°		OA209

$$\frac{c_{d, \text{tip}}}{c} = 0,15$$

$$\frac{c_{d, \text{tip}}}{c} = 0,25$$

$$\frac{c_{d, \text{tip}}}{c} = 0,6$$

Fig.3. - Rotor blades definition

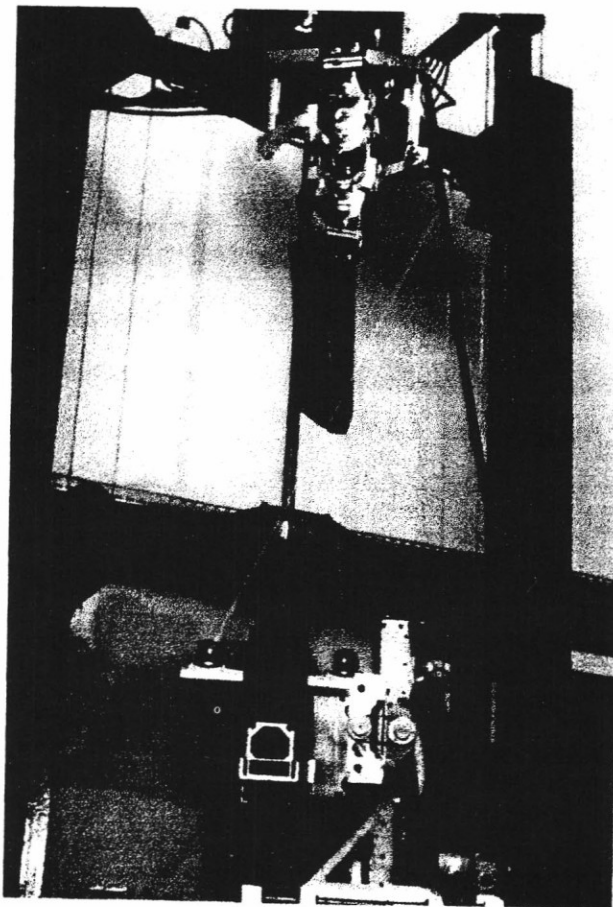
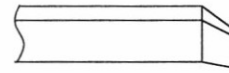
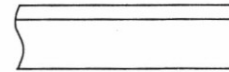
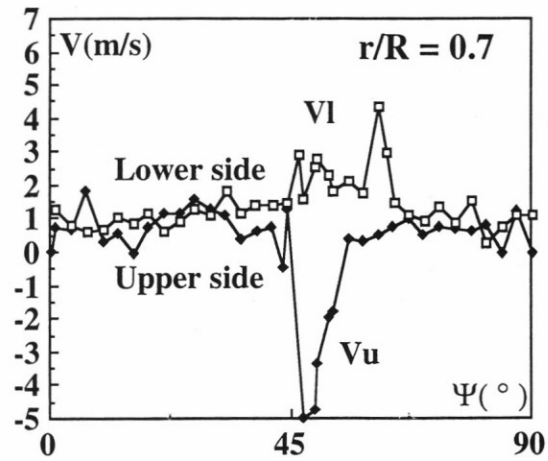


Fig.4. - Laser velocimetry system



ROTOR 4



ROTOR 7

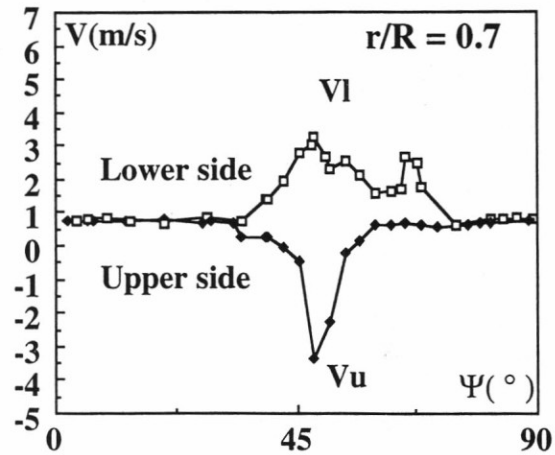
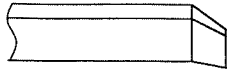
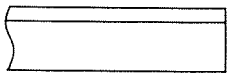
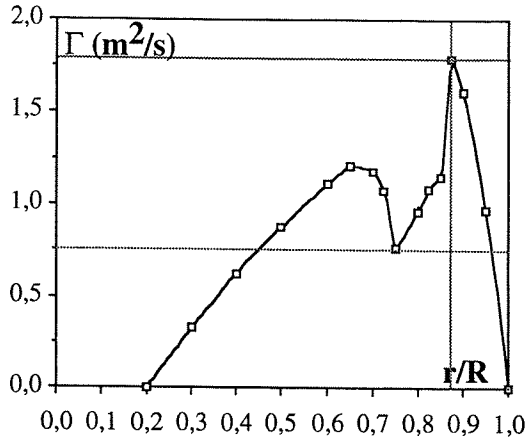


Fig.5. - Tip shape influence on tangential velocity field



ROTOR 4



ROTOR 7

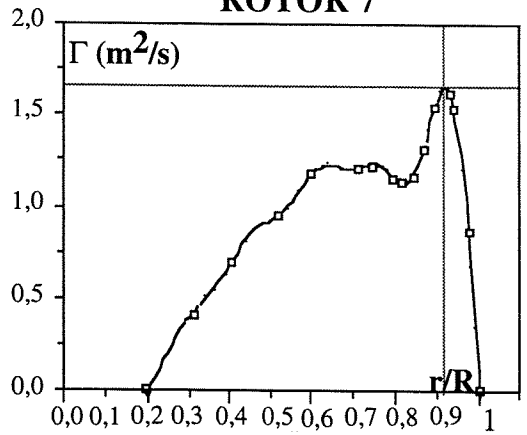


Fig.6. - Tip shape influence on circulation distribution along the blade span

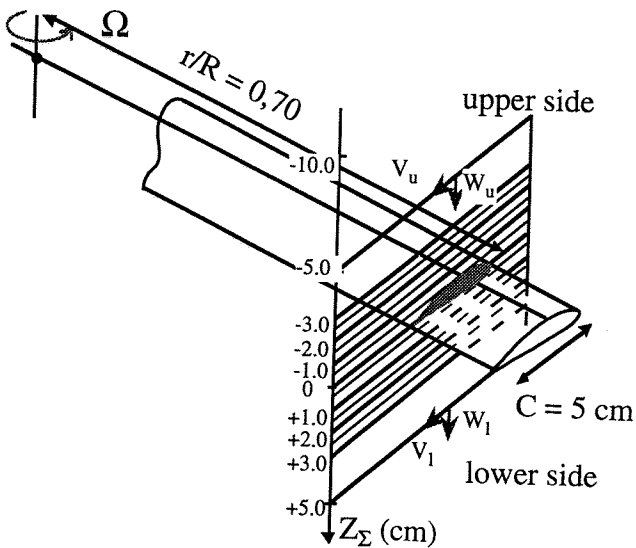
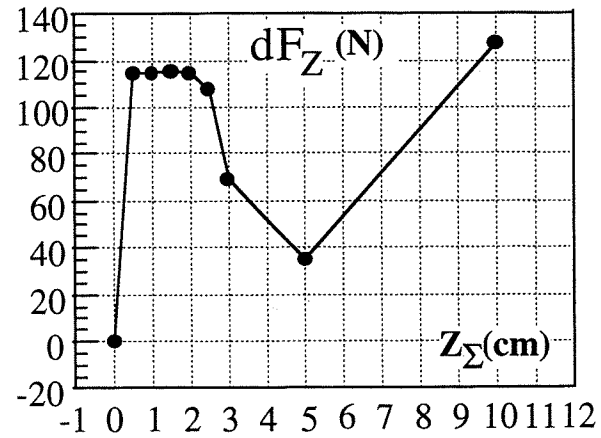
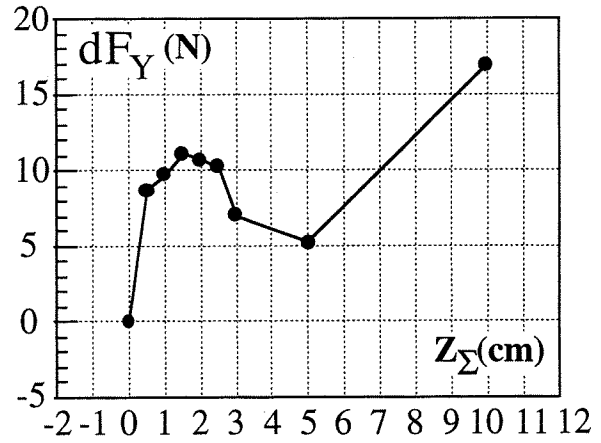


Fig.7. - Selection of the contour thickness Z_{Σ}



$$|Z_{\Sigma}| < 2.5 \text{ cm}$$

Fig.8. - Influence of the integrating contour Z_{Σ}

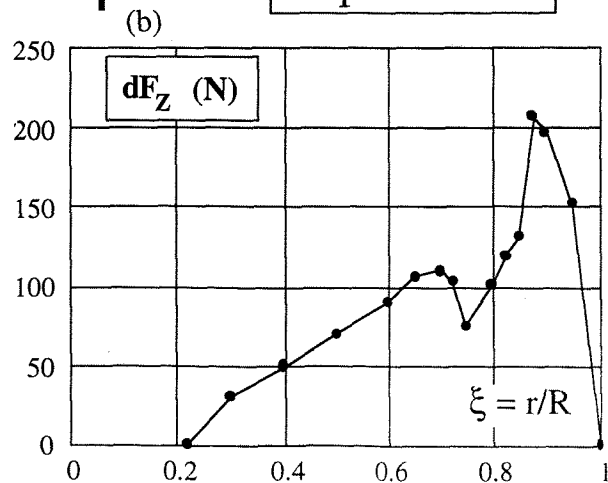
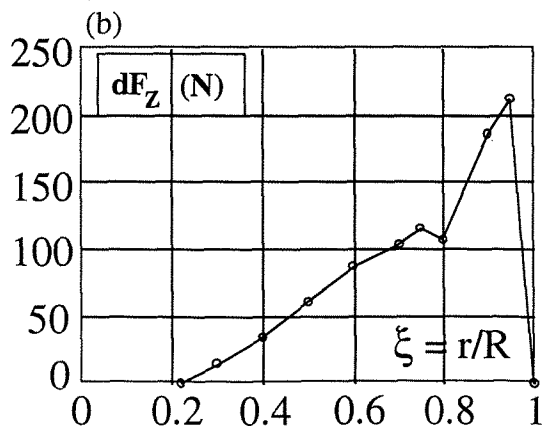
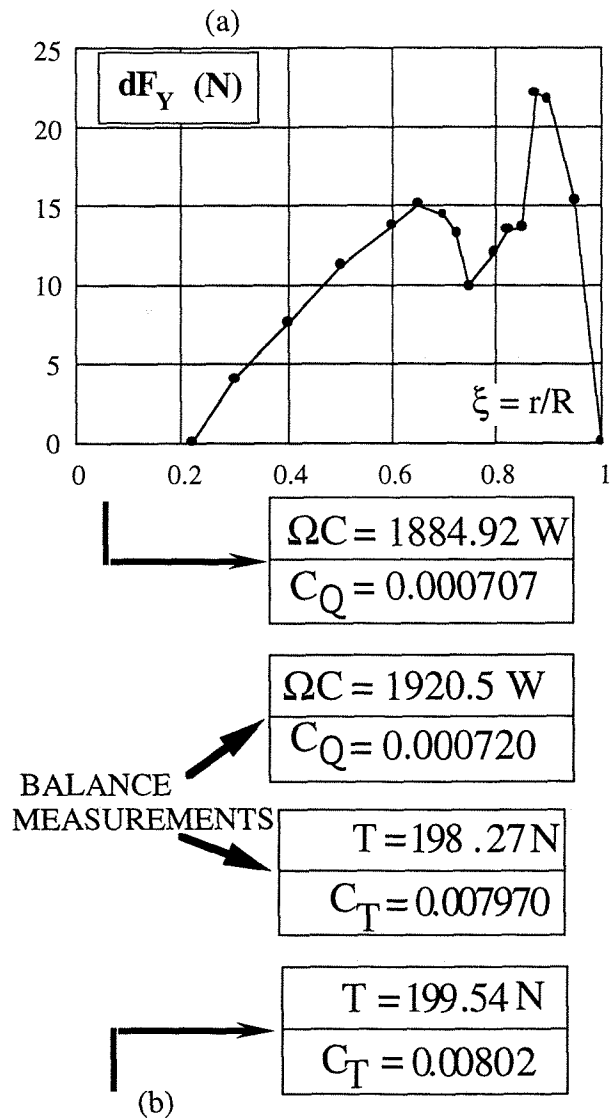
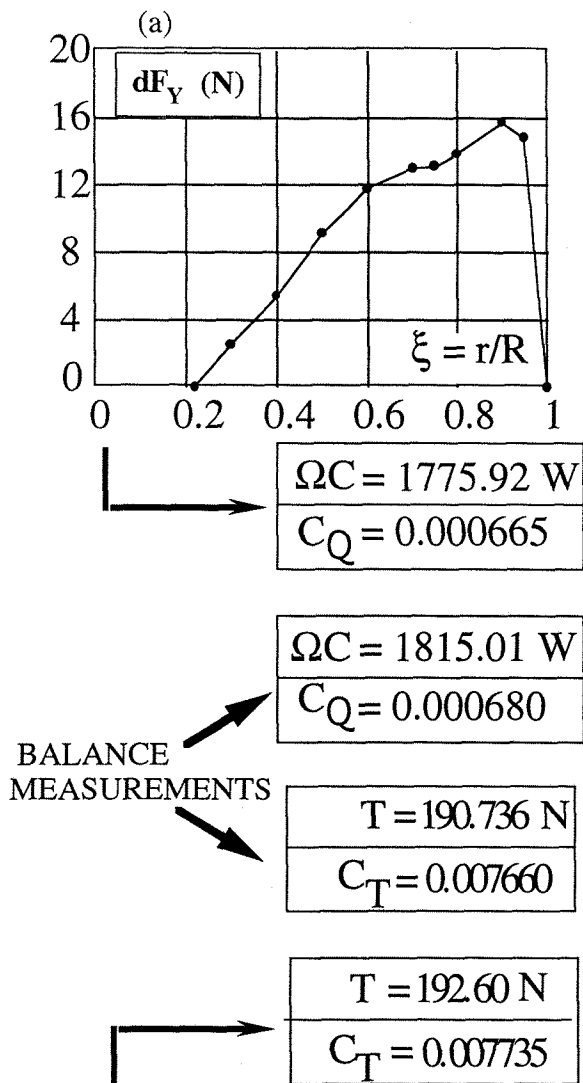


Fig.9. - Spanwise evolution of the elementary forces (rotor 7, $b = 4$, $\theta = 10^\circ$)

Fig.10. - Spanwise evolution of the elementary forces (rotor 4, $b = 4$, $\theta = 10^\circ$)

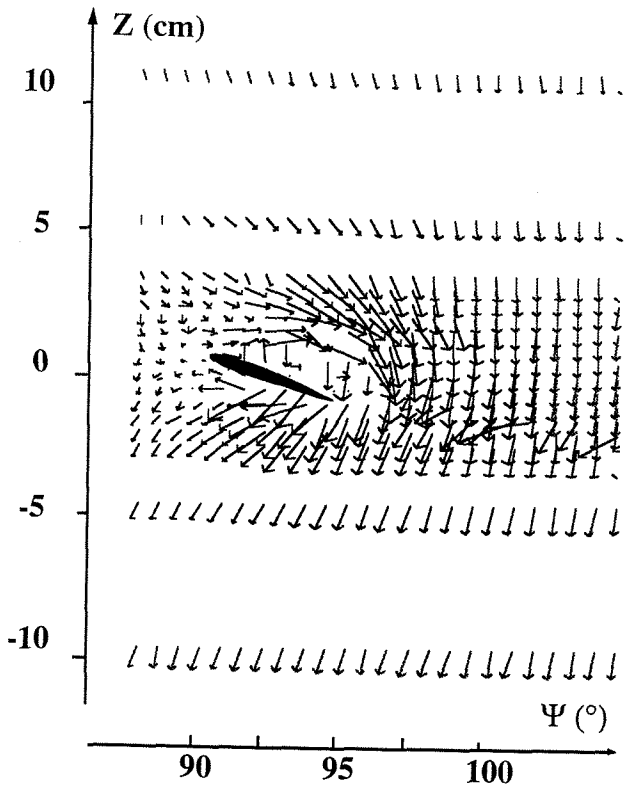


Fig.11. - Induced velocity field, $r/R = 0.75$,
(rotor 7, $b = 4$, $\theta = 10^\circ$)

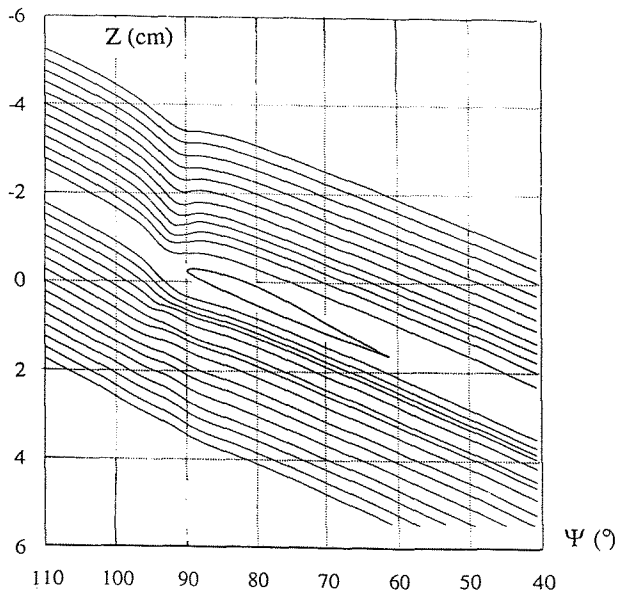
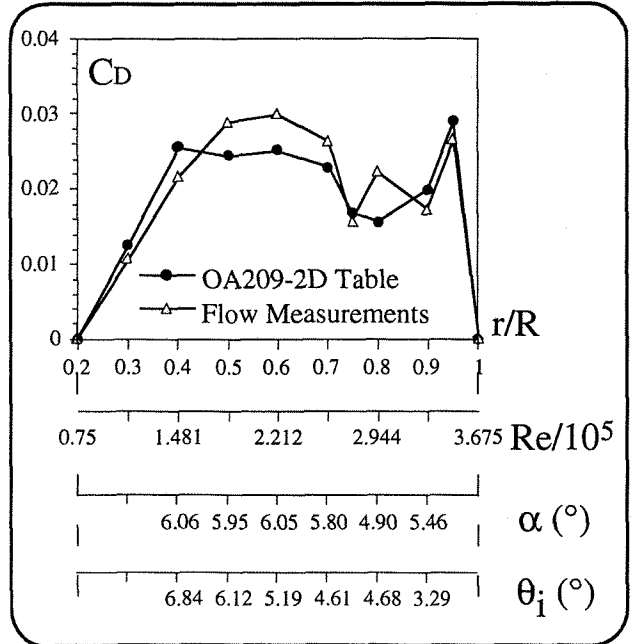
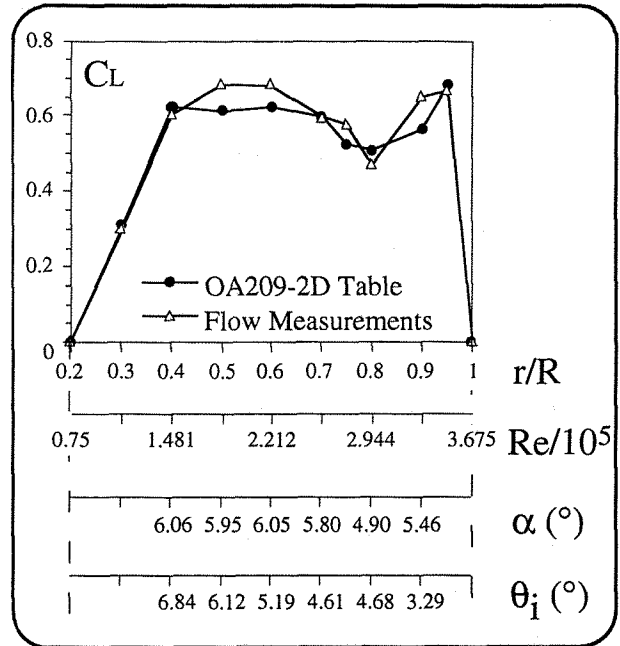


Fig.12. - Streamlines around the blade section
, $r/R = 0.75$, (rotor 7, $b = 4$, $\theta = 10^\circ$)

Fig.13. - Comparison on (C_L , C_D) deduced from L.V. measurements and OA209 2D-tables, (rotor 7, $b = 4$, $\theta = 10^\circ$)